Improving the design of atomic magnetometer arrays for RF interference mitigation in NQR detection of explosives

Robert J. Cooper[a], Brian L. Mark[b], David W. Prescott[a], and Karen L. Sauer[a]

George Mason University, Fairfax, VA, U.S.A.
[a]Dept. of Physics and Astronomy;
[b]Dept. of Electrical and Computer Engineering

ABSTRACT

Nuclear Quadrupole Resonance (NQR), a type of radio frequency spectroscopy, holds the promise of unambiguous detection of particular explosives; the associated resonant frequencies are virtually unique. This specificity is spoiled by natural and anthropogenic interference that can swamp the NQR signal. Fortunately, the spatial magnetic signature from the explosive differs significantly from that of interference and can be exploited to separate the signals. An array of coils, however, cannot provide truly independent measurements due to the inductive coupling between the coils. Single coil configurations can cancel out constant interference and retain the signal from an NQR coil, but the balance between arms of the coil is compromised by differential coupling to the environment. Atomic magnetometers, an emergent technology predicted to surpass the sensitivity of coil detection, do not suffer from such coupling and have no fundamental limitation to forming an array of independent sensors. We have demonstrated up to 94× interference rejection with a 4-sensor array spanning 25 cm. The array symmetry permits rejection of linearly varying interference. We discuss the prevention of reradiation from DC field coils used to set the magnetometer resonance frequency. Such reradiation leads to non-linear variation. The benefits of larger sensor arrays are also explored.

Keywords: Explosives detection, Nuclear Quadrupole Resonance (NQR), atomic magnetometers, radio-frequency interference mitigation, array of magnetometers, unshielded detection

1. INTRODUCTION

Nuclear quadrupole resonance (NQR) can provide definitive detection of explosives[1–3] since the explosive has a unique radio-frequency (RF) signature according to its crystalline structure and quadrupolar nuclei,[4] for instance ^{14}N, ^{35}Cl, ^{79}Br, ^{81}Br, and ^{39}K. The signal, however, tends to be somewhat weak due to the relatively low frequencies of the spectra. Standard coil detection relies on Faraday induction and therefore the voltage induced is proportional to frequency. The atomic magnetometer's signal is relatively independent of frequency and is therefore fundamentally more sensitive than that of a coil at the lower frequencies required for explosives detection.[5]

Furthermore, the magnetometers do not inductively couple to one another, unlike coils in an array, and therefore can provide truly independent measurements of the magnetic field allowing for a spatial map of the RF field distribution. Magnetometers also do not capacitively couple to the environment, and therefore do not experience the same imbalancing that a single coil multi-turn gradiometer experiences.[6] A simple four-sensor array can be used to reject interference that varies linearly in space.[7] The main limitation to interference rejection is scattering from the system's DC field coils that are used to set the magnetometer resonance frequency. We have designed and implemented a set of field coils that minimizes this scattering, resulting in improvement in the rejection of interference by more than a factor of two from previous results.[7]

In order to achieve a similar volume of detection as for a coil, a larger sensor array than four is required. We discuss the design of an eight-sensor array for the rejection of interference and detection of the volume under an excitation coil of radius $R = 10$ cm. Signals from both large and small explosives are treated.

Further author information: (Send correspondence to K.L.S.)
K.L.S.: E-mail: ksauer1@gmu.edu

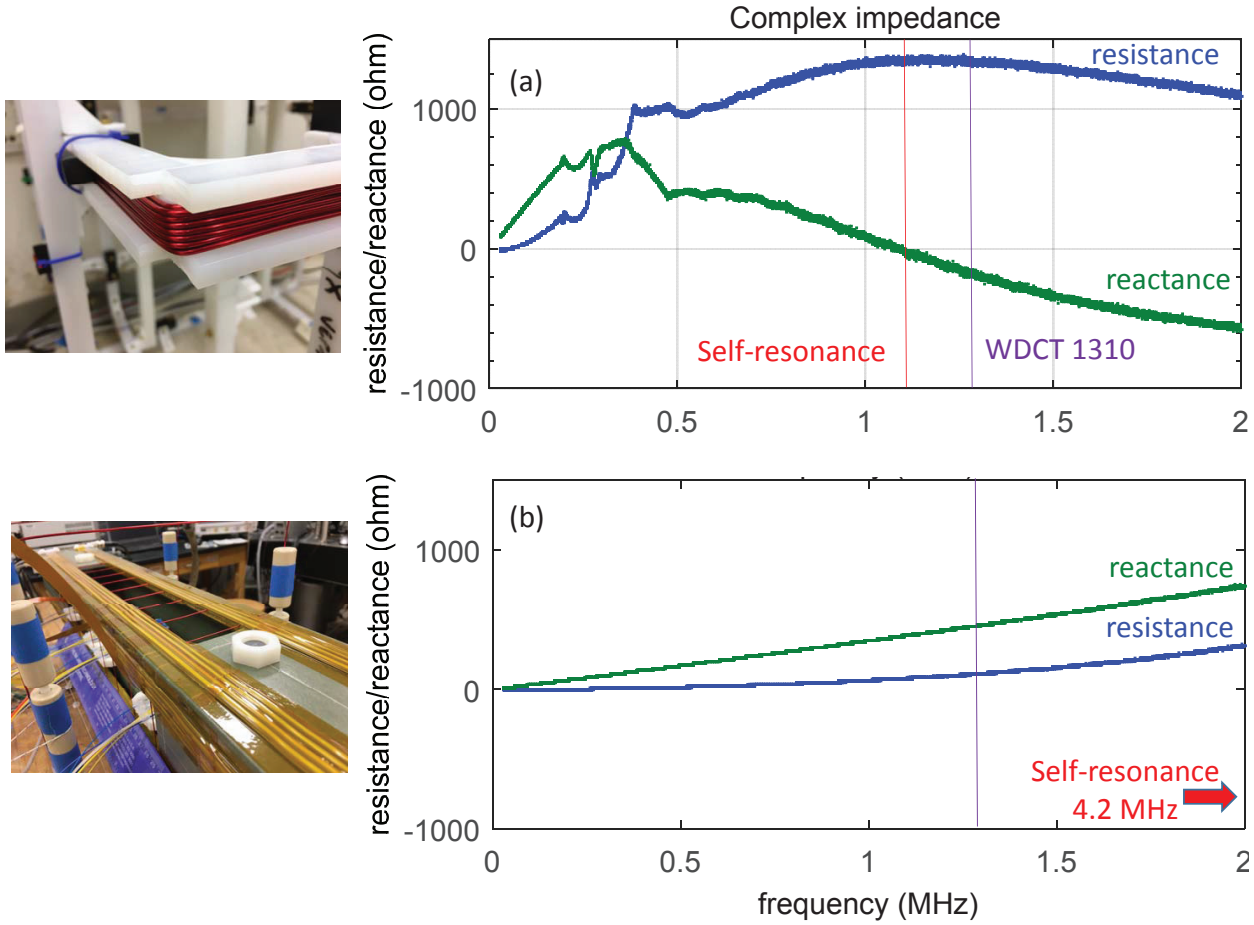

Figure 1. Capacitance between loops in the original design in Ref. 7, shown in the upper left, leads to a self-resonance close to the frequency to be rejected from the local radio station WDCT 1310, (a). By using ribbon wire for the field coils, lower left, loops are displaced from each other, reducing capacitance between loops and moving the resonance away from the interference frequency, (b). The optical fibers from the four sensors can be seen sticking out of the 4 × 4 inch fiberglass tube around which the coils are wrapped.

The remainder of the paper is organized as follows. In Section 2, we describe the experimental setup of the magnetometer sensor array system. In Section 3, we discuss a method for real-time calibration of the arrays. In Section 4, we discuss the interference rejection properties of the system. In Section 5, we discuss the optimal placement of the sensors to minimize the interference. The paper is concluded in Section 6.

2. EXPERIMENTAL SETUP AND RERADIATION OF INTERFERENCE

The experimental setup used in this work is quite similar to that described in Ref. 7. We will therefore focus on the differences from that setup. The fiber-coupled sensors, made by Twinleaf,[8] are operated in a crossed pump-probe configuration. The pump laser is resonant with the D1 line of the ^{87}Rb atoms, and is 2 orders of magnitude higher in power than the probe laser. The probe power is on average 2.9 mW in the fiber before the cell and 0.74 mW as measured after the exit from the cell and at the photodiodes. The probe wavelength is off-resonant from the D1 line by $\Delta\lambda = 0.12$ nm. The sensor sensitivities ranged from 14-25 fT/$\sqrt{\text{Hz}}$, but it should be noted that minimal effort was made to optimize the sensitivity for these experiments.

The four magnetometers are arranged in a line at distances of $[-12.5 \quad -2 \quad 2 \quad 12.5]$ cm. The two inner sensors are meant to measure the signal of interest, while the two outer sensors measure the interference. As explained in more detail later (see Section 5), subtracting the received signals at the outer sensors from those

at the inner sensors removes the effect of the component of interference that varies linearly with respect to displacement.

The interference will be approximated more closely by the linear component the closer the exterior sensors are to each other. This effect can be estimated by looking at the j^{th} component of the magnetic field from an oscillating magnetic or electric dipole placed at the origin:[9]

$$B_j(k\mathbf{r}) = \sum_{m=1}^{3} A_m \frac{e^{-ikr}}{(kr)^m} f(\hat{r}), \tag{1}$$

where $\mathbf{r}$ is the displacement from the origin and $f(\hat{r})$ is a function only of the unit vector $\hat{r}$. All distances are scaled by k, the wavenumber. For multiple sensors spaced at a distance $\mathbf{a}$ from the center of the excitation coil $\mathbf{r}_c$, we can use the Taylor series expansion to expand the above function as follows:

$$B_j(k\mathbf{r}_c + k\mathbf{a}) = B_j(k\mathbf{r}_c) + k\mathbf{a} \cdot \nabla_{k\mathbf{r}} B_j|_{k\mathbf{r}=k\mathbf{r}_c} + \frac{1}{2} k_0^2 \mathbf{a} \cdot \left[\mathbf{a} \nabla_{k\mathbf{r}} \left(\nabla_{k\mathbf{r}} B_j\right)\right]_{k\mathbf{r}=k\mathbf{r}_c} + \cdots . \tag{2}$$

The first term represents a constant over all the sensors, the second a linear term, etc. The second term has components of order $k_0 a \left(\frac{1}{k_0 r}\right)^m$ and $\left(\frac{a}{r}\right)\left(\frac{1}{k_0 r}\right)^m$. The third term has components of order $(k_0 a)^2 \left(\frac{1}{k_0 r}\right)^m$, $k_0 a \left(\frac{a}{r}\right)\left(\frac{1}{k_0 r}\right)^m$, and $\left(\frac{a}{r}\right)^2 \left(\frac{1}{k_0 r}\right)^m$, and so forth. Therefore, for $a \ll r$ and $k_0 a \ll 1$, the fields will be linear. The latter requirement is quite reasonable for radio frequencies. The former largely will depend on the closeness of the radiation source with respect to the spatial extent. Keeping this in mind, the quadratic component will roughly be a factor of $\frac{a}{r}$ smaller than the linear term, which shows that the quadratic component becomes smaller the closer the sensors are placed. The quadratic term is not completely eliminated in the proposed scheme.

In fact the main hinderance to interference rejection in the setup of Ref. 7 was the strong presence of a quadratic component. In some configurations, the quadratic component was close to 30% of the signal, and of the same order of magnitude as the linear component. Given Eq. 2, and $k_0 a \sim 0.003$, a large quadratic component in comparison to the linear term would occur when the ratio $\frac{a}{r}$ is significant, meaning that the source of radiation was close. This would occur if the interference is reradiated from a local source. The most local of sources are the field coils surrounding the sensors, although the optics table, which was 0.6 meters below the array in the original configuration, would be a close second. Notably, we found that the some of the field coils were self-resonant at frequencies close to that of a local radio station, see Fig. 1a.

Because of the capacitance c between loops, current would be allowed to flow in response to the changing flux caused by the interference, in other words, reradiation of the field would occur. When ω increases through the resonance condition $1/(\ell c)$, where ℓ is the inductance per loop, the phase of the impedance changes from positive to negative and the resistance peaks, as observed in Fig. 1a. The inductance per turn of the field coil can be reduced by decreasing the size of the loops, whereas the capacitance can be reduced by moving the wires farther apart. In this way, new field coils were designed to have the self-resonance frequency moved much higher than that of the radio station, see Fig. 1b. Ribbon wire was used to enforce the displacement of the wires and coils were formed on a 4×4 inch fiberglass tube, 0.7 m in length.

3. CALIBRATION

For accurate detection, and therefore accurate interference mitigation, the sensors are calibrated in real-time by applying a known field to the sensor. A pair of 21×21 cm square coils are placed to give equal excitation over the four sensors. The strength of the calibration field B_c used in the following data was 14.4 pT, but much higher values can in principle be used as long as the spin system is not RF broadened,[10] that is,

$$B_c \ll \frac{1}{\gamma \sqrt{T_1 T_2}} \sim 10 \text{ nT}, \tag{3}$$

where γ is the ^{87}Rb gyromagnetic ratio, T_1 is the spin-lattice, and T_2 the spin-spin time constants. Here, B_c is determined by varying the excitation strength while keeping the duration t_p fixed; the resulting signal is

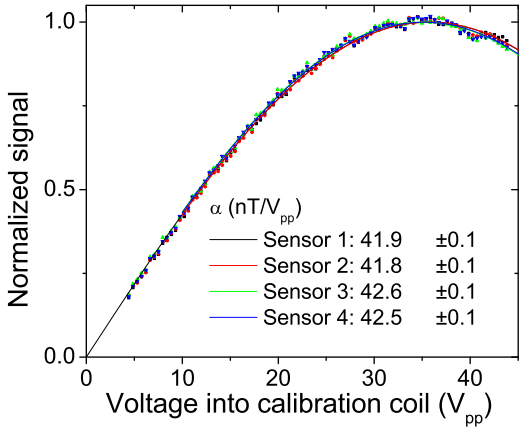

Figure 2. The signal following a resonant RF pulse of duration 47.8 μs has a sinusoidal dependence on the strength of the calibration field. By fitting the data, the field for a given input voltage, α, is determined.

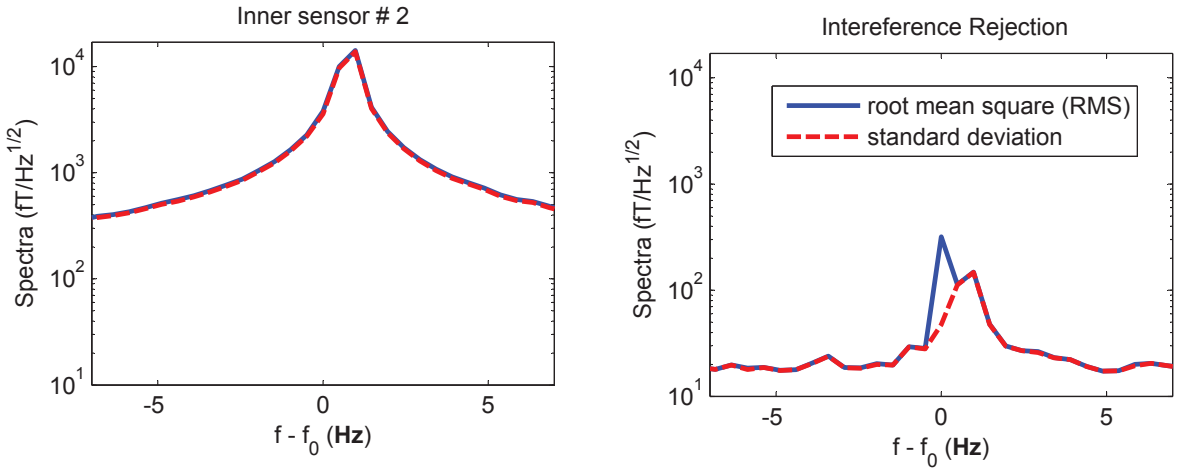

Figure 3. With just a single sensor, the interference dominates the 38 times smaller signal, left hand graph. By using all four sensors, and the interference rejection algorithm, the signal is revealed and the interference is rejected by a factor of 94 at its peak, right hand graph. The standard deviation, dashed red lines, is a measure of the noise, while the root-mean-square, solid blue lines, includes the signal.

proportional to $\sin \frac{\gamma \alpha V_{\rm in} t_p}{2}$, where $\alpha = B_c/V_{\rm in}$ is the ratio between B_c and the voltage $V_{\rm in}$ into the probe, see Fig. 2.

In addition to an amplitude, a phase is also associated with the calibration field. The field coil is designed to give a field in only one direction $\hat{x}$ over all four sensors. However, due to placement of the sensors there may also be a small $\hat{y}$ component which would register as a phase shift, $\phi \approx B_y/B_x$. To make a clean measurement of this phase, a short strong resonant pulse is applied to the sensors through the calibration coil, and the phase of the resulting signal is measured. Optical read-out electronics also contribute to the observed phase and must be measured separately. Deviations in phase, 5 degrees or less, were observed from both electronic and field sources. With the strength and phase dependence of the calibration signal determined, the real-time calibration data can be used to correct the signal on the fly.

4. INTERFERENCE REJECTION

Interference at the carrier frequency of a local radio station, 1.310 MHz, of 14 $\rm pT_{rms}$, is measured with one orientation of the array; this orientation is denoted $\parallel$. When the array is rotated by 90 degrees, denoted the $\perp$ orientation, the signal is measured to be 1.8 $\rm pT_{rms}$. The sensors measure fields in a 2D plane orthogonal to the

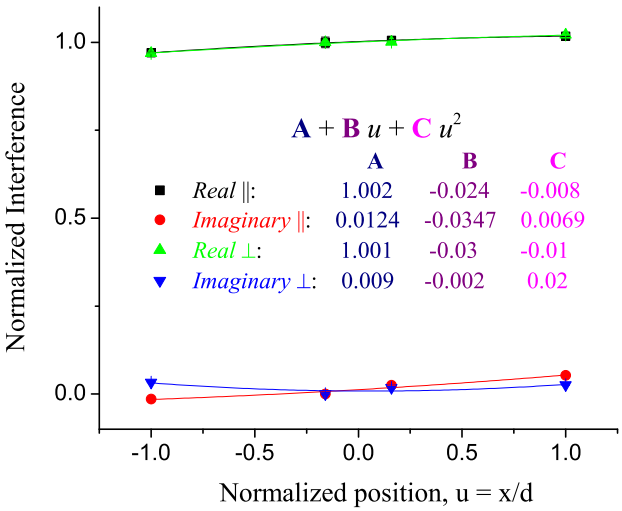

Figure 4. The interference is plotted as a function of distance, scaled to the farthest sensor position, $d = 12.5$ cm, from the center. The fit shows the relatively small quadratic contribution to the in-phase (real) and out-of-phase (imaginary) components of the interference, for both orientations of the magnetometer array. The interference algorithm only cancels the constant and linear terms.

static field that creates the resonance, so with rotation of the array, and the static field along with it, different field directions are measured.

In the $\parallel$ orientation, using the sensor array and interference algorithm, the interference suppression varies over time, but lies between 50-100, see Fig. 3. In the $\perp$-direction the interference suppression lies between 30-50. This represents more than a factor of two improvement over our previous results, Ref. 7. The key differences are in the reduction of the reradiation footprint of the field coils, the removal of the optics table upon which the former experiment rested, and a careful analysis of the phase of the calibrations signal. All three contributions lead to a reduction in the quadratic component of the interference signal with distance over the sensors, see Fig. 4. The reduction in quadratic component was between 2-4 for the $\parallel$ direction and 10-30 for the $\perp$ direction. The remaining quadratic component, which is 1-2% of the total interference signal is what limits the rejection ratio. The array sits in the lab about 2 meters from a large, 3×1.2 m, optics table; the long edge of the table is parallel to the array when the array is in the $\perp$ orientation. Reradiation from this table may be responsible for the residual quadratic component.

The signal in Fig. 3 is created by a small 2-turn coil of diameter 2 cm. The coil is centered on the array and placed 5 cm above it. Therefore, the outer sensors are 2.5 times further away from the coil compared to the inner sensors. The signal at the outer sensors should be less than 7% of the signal at the inner sensors. The size of the field is 380 fT at the inner sensors. An interference reduction algorithm is applied, which takes half the sum of signals from the inner sensors minus the sum of the signals from the outer sensors. After the interference algorithm, the size of the signal is reduced to 95% of its original value. Without the presence of the interference, the size of the noise is typically a bit lower after the interference algorithm is applied. Therefore, in comparison to using a single sensor, use of the magnetometer array preserves the SNR. In the presence of interference, the SNR is improved by the rejection ratio.

5. OPTIMIZING SENSOR PLACEMENT

The sensors can be placed in a configuration that minimizes the effect of interference. If the sensors close to the explosive are placed in a symmetric pattern about the center of the coil, summing their received signals will cancel the first-order component of the interference that varies linearly with displacement from the center. To eliminate the constant component of the interference, while avoiding reintroducing the linear component, another set of sensors can be placed symmetrically around the center of the coil, but further away from the explosive and exterior to the coil. Summing the signals from the exterior sensors will eliminate the linear component and

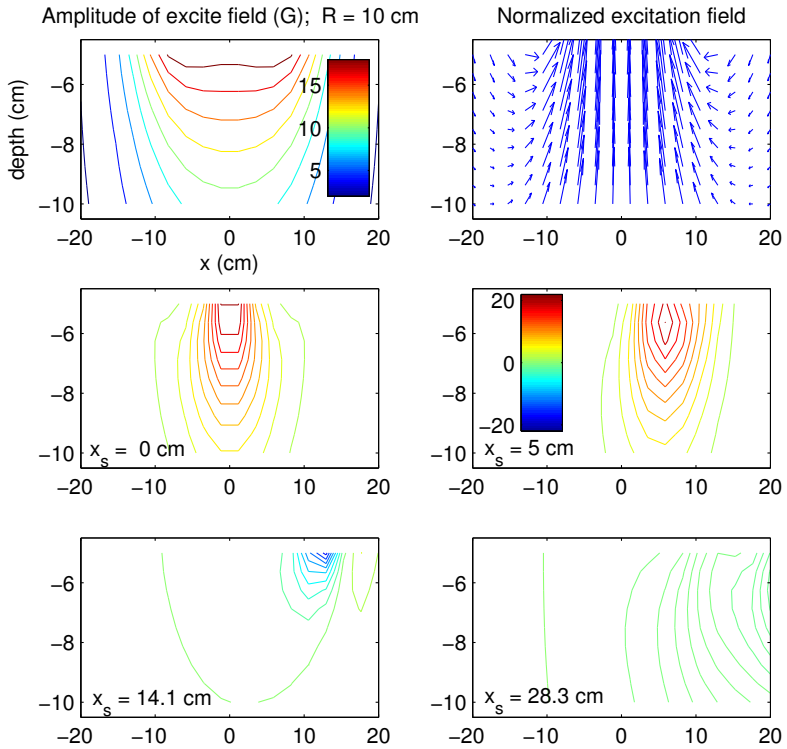

Figure 5. The amplitude, top left graph, and direction, top right, of the excitation field are shown. As shown in the middle and bottom graphs, the region of sensitive detection varies depending on the horizontal placement of the magnetometer sensor, x_s. The magnetometers are placed in the same plane as the coil. The graphs show the NQR field measured at the sensor for a 200 g spherical sample of ammonium nitrate placed at different depths and horizontal displacement, x. Note that for the sensors placed at $\sqrt{2}R$ (left bottom) and $2\sqrt{2}R$ (right bottom) the signal from the central space is negative. Therefore, when the signal from this exterior magnetometer is subtracted out, the net signal increases.

leave the constant component. By then subtracting the sum of the signals from the exterior sensors from the sum of the signals from the interior sensors, both the constant and linear components of the interference can be removed. There may be a temptation to use fewer exterior sensors and to focus attention on interior sensors, which receive the bulk of the desired signal. However, the interference must be handled carefully to avoid the presence of a high level of noise in the final processed signal.

The noise in the received signals from the sensors add in quadrature if the signals are weighted equally. However, some of the sensors can be assigned more weight than others, for example, if the number of exterior sensors, N_e, is less than the number of interior sensors, N_i. In this case, the noise added to the final signal would be weighted by the factor $\alpha = N_i/N_e$. Instead of noise power growing as $\sqrt{N_e}$ for incoherent noise in the exterior sensors, the noise power grows as $\alpha\sqrt{N_e}$. For a fixed number of sensors $N = N_i + N_e$, and assuming only the interior sensors add to the signal, the signal-to-noise ratio satisfies

$$\mathrm{SNR} \propto \left(\frac{1}{N_i} + \frac{1}{N - N_i} \right)^{-1/2} . \tag{4}$$

The right-hand side of Eq. (4) is maximized as a function of N_i when $N_i = N_e = N/2$.

Assuming, therefore, that $N_e = N_i$, the sum of signals from the exterior sensors is simply subtracted from the corresponding sum from the interior sensors. Ideally, there would be no loss of signal from the explosive in performing this subtraction. The field from the explosive is approximately the same as that from a magnetic dipole $\mathbf{m} = m\hat{y}$,

$$\mathbf{B}_{dip}(\mathbf{r}) = \frac{\mu_0}{4\pi r^3} \left[3(\mathbf{m} \cdot \hat{r})\hat{r} - \mathbf{m} \right] , \tag{5}$$

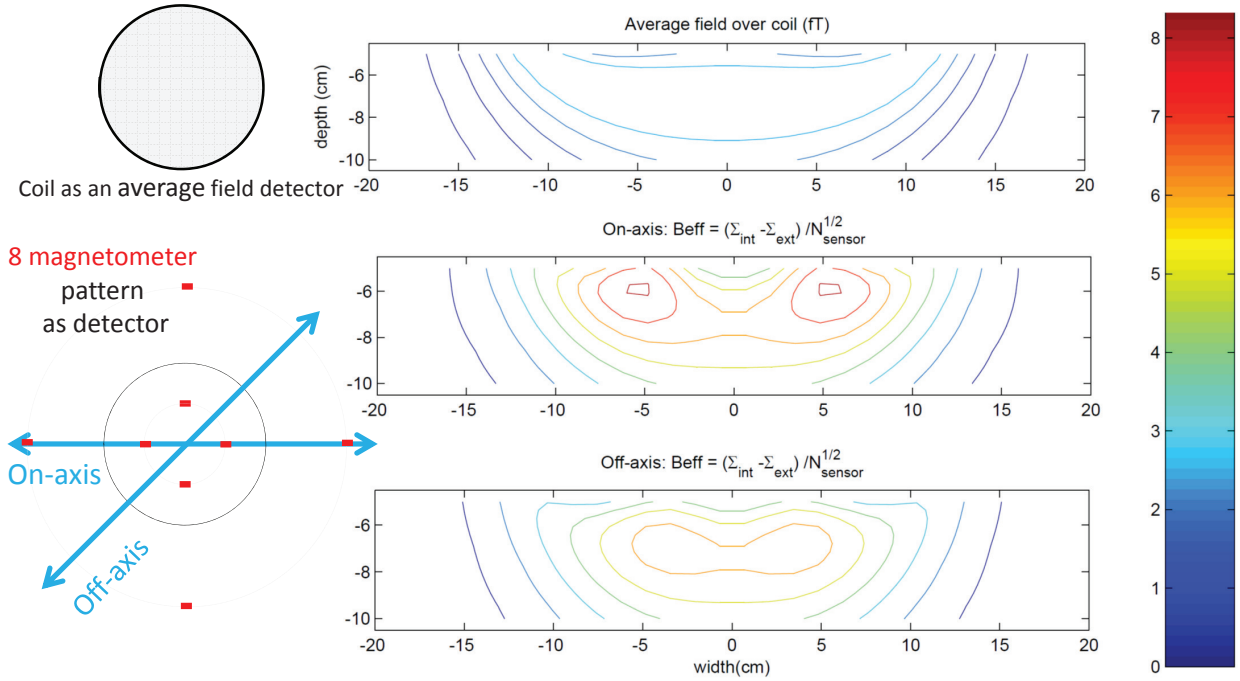

Figure 6. The detected signal from a 200 g spherical sample of ammonium nitrate, using a coil, is proportional to the average field over the coil, top graph and schematic. By comparison, the placement of eight sensors, shown as red squares in the bottom schematic, gives a net signal from explosives on axis (center graph) and off-axis (bottom graph). The colorbar shows the range in fT used over all three graphs. For easier comparison, Fig. 7 shows the ratio of B_{eff} to $\bar{B}_{\text{coil}}$.

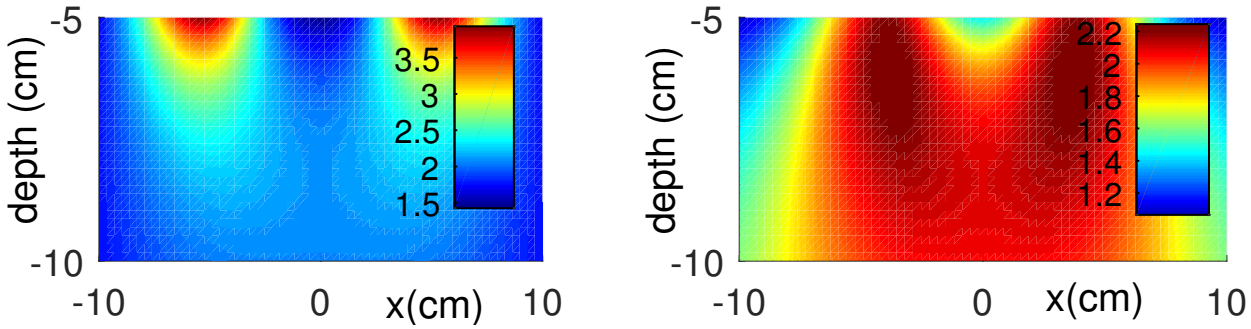

Figure 7. Ratio of B_{eff} to $\bar{B}_{\text{coil}}$ from on-axis (left) and off-axis (right) configurations. In all cases, the signal detected by the magnetometer is equal to or exceeds that detected by the coil.

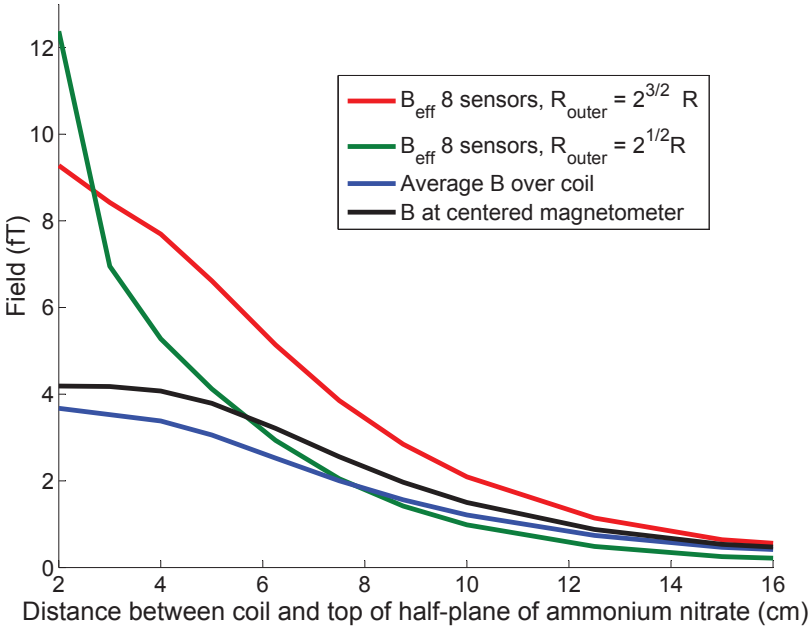

Figure 8. The detected signal in fT from a half plane of ammonium nitrate at various distances below the excitation coil plane, $R = 10$ cm. The signal size for a coil (black) and one centered magnetometer (blue) asymptotically approach one another the deeper the explosive is buried, as is to be expected. When adding in the sensors for interference rejection, having the outer sensors closer (green, $R_{\text{outer}}/R = \sqrt{2}$, red, $R_{\text{outer}}/R = 2\sqrt{2}$) is beneficial for surface explosives but detrimental for deeper explosives.

where $\mathbf{r}$ is the displacement from the explosive to the sensor and μ_0 is the permeability of free space. The y-field component of the field,

$$B_y(\mathbf{r}) = \frac{\mu_0 m}{4\pi r^3}\left[3\cos^2\theta - 1\right], \tag{6}$$

reverses direction depending on θ, the angle between the y and $\hat{r}$. The angle at which the expression in square brackets is zero is called the magic angle,

$$\theta_m = \arccos\frac{1}{\sqrt{3}} = 54.7\,\text{deg}\,. \tag{7}$$

For $\theta < \theta_m$, the B_y field is positive; for $\theta > \theta_m$, it is negative. It is for this reason that a large coil as a sensor is at a disadvantage for detecting small samples that are close to it - some of the flux through the coil becomes negative and cancels out the positive flux. For the magnetometer array, the interior sensors should be placed such that $\theta < \theta_m$. This requirement is the most stringent for those explosives closest to coil, at a depth d_{min} away. Ideally there should be at least one sensor within a horizontal distance $l \ll \sqrt{2}d_{\text{min}}$ of these close explosives to satisfy the condition $\theta < \theta_m$. For the magnetometers, this requirement will guide the number and placement of the interior sensors. In a similar manner, d_{min} will end up restricting the radius of the detection/excitation coil in conventional detection. For a sample calculation, a 200 g spherical sample of ammonium nitrate is taken, radius $r_s = 3$ cm, and a stand-off distance of 2 cm assumed; therefore, $d_{\text{min}} = 5$ cm. The radius of the coil is taken as $R = 10$ cm, and the four interior sensors are spaced symmetrically at a radius of $R/2$.

In contrast, an exterior sensor should be placed such that $\theta > \theta_m$ so that any field produced by the explosive at the sensor will add to, instead of subtract from, the final signal after signal processing. For a deep explosive at the distance d_{max} below the excitation coil plane, the exterior sensors should be placed at a distance $\geq \sqrt{2}d_{\text{max}}$ from the center. Under this condition, closer explosives to the coil will automatically comply with $\theta > \theta_m$. A coil of radius R roughly addresses a volume that extends down to a distance R into the volume of inspection, see Fig. 5. The size of the magnetization M induced in the explosive depends on the strength of the excitation

field. For example, for a ^{14}N-containing sample at temperature T, with NQR frequency f and n resonant nuclei per volume,

$$M = n\mu \left[\frac{hf}{3kT}\right] \left[\frac{\sin\phi - \phi\cos\phi}{\phi^2}\right], \tag{8}$$

where ϕ is that the angle of excitation and is directly proportional to the excitation field B_1; the constants are Planck's constant h, Boltzmann's constant k, and μ is the magnetic moment for one nucleus. To avoid having any nulls in detection, $\phi < 4.5$ rad for the region of interest. Assuming a 100 μs-long RF pulse, the excitation field is chosen to equalize the signal from the coil at the top and bottom of this region for detection by a coil, see Fig. 6.

As shown in Fig. 6, a pattern of eight sensors, four placed at $R/2$, and four placed at $2R\sqrt{2}$ gives a comparable addressed volume as the detection of magnetic flux by the coil. The signal regions for the individual sensors are shown in Fig. 5. For the eight sensor pattern, the effective field is taken as the sum of the interior signals minus the sum of the exterior fields, divided by the square root of the number of sensors. This normalization takes into account the $\sqrt{N}$ increase in base noise, anticipating uncorrelated noise across the sensors. Taking as the region of interest the diameter of the coil, the net magnetometer signal is between 1.4 in the middle to 3.9 at surface hot spots more than the coil signal for the on-axis case, and between 1 on the far edges and 2.2 in the interior for the off-axis case, see Fig. 7. A larger number of sensors and a more sophisticated data processing scheme could yield more uniform sensitive coverage as well as localization information.

The calculations described above are for relatively small explosives. We can get an estimate for a large sample by creating a mesh of dipole moments throughout the half space starting at various distances below the excitation coil. The results are shown in Fig. 8. Calculations for $R_{\text{outer}} = \sqrt{2}R$ and $R_{\text{outer}} = 2\sqrt{2}R$ are done for comparison, the former being better for interference rejection. While the choice of $R_{\text{outer}} = \sqrt{2}R$ gives a better signal response closer to the surface, as shown in Fig. 8, the choice of $R_{\text{outer}} = 2\sqrt{2}R$ gives a better signal for deeper samples. With placement of the outer sensors at $2\sqrt{2}R$ away from the center, the signal from the array is greater than that of the coil even for deep explosives.

The atomic magnetometers used here are quite compact with an active volume of 0.36 cm^3. In addition the probe beam only passes through the active volume twice. In this configuration the noise is fundamentally limited by photon shot noise[7] and sensitivity between 14-25 fT/$\sqrt{\text{Hz}}$ is observed. With an order of magnitude more passes, an order of magnitude better sensitivity has been obtained.[7] By controlling for non-fundamental noise sources,[11] increasing the cell-size by an order of magnitude,[12] and using potassium instead of ^{87}Rb,[13] sensitivity should improve by another order of magnitude, make it comparable to sensitivity seen with a much larger cell size 100 cm^3.[14] Taking a projected sensitivity of 0.25 fT/$\sqrt{\text{Hz}}$, and considering the decrease in signal over an echo train,[15] the half-plane of ammonium nitrate, Fig. 8, at a distance of 10 cm away, should give an SNR of 5 for a single 4 s long echo train and detection by the 8-sensor array. The signal size from this large sample is comparable to that of the 200 g sample placed at 10 cm deep and off-center by 10 cm, Fig. 6. Therefore a similar SNR and scan time would be expected.

6. CONCLUSION

With relatively straightforward changes to our previous experimental setup in Ref. 7 we were able to increase interference rejection by more than a factor of two. Interference rejection close to a factor of 100 has been observed, and is most likely limited by local sources of reradiation.

By doubling the number of sensors from four to eight, the volume of detection should match that of a coil. Our calculations show that the signal from some places within that volume can exceed that measured by a coil by more than a factor of 3. With careful placement of the sensors, the enhancement in signal translates to larger samples, shallow or deep. The potential order of magnitude decrease in noise would only multiply these gains, see Ref. 5. Therefore, atomic magnetometers arrays hold the promise of sensitive detection with strong interference mitigation.

ACKNOWLEDGMENTS

The authors would like to thank the College of Science, the Volgenau School of Engineering, and the Department of Physics and Astronomy at George Mason University for providing seed funding for this multidisciplinary work. This work was also supported by DARPA Contract No. HR0011-13-C-0058.

REFERENCES

[1] Garroway, A. N., Buess, M. L., Miller, J. B., Suits, B. H., Hibbs, A. D., Barrall, G. A., Matthews, R., and Burnett, L. J., "Remote sensing by nuclear quadrupole resonance," *IEEE Transactions on Geoscience and Remote Sensing* **39**, 1108–1118 (Jun 2001).

[2] Miller, J. B. and Barrall, G. A., "Explosives detection with nuclear quadrupole resonance: An emerging technology will help to uncover land mines and terrorist bombs," *American Scientist* **93**(1), pp. 50–57 (2005).

[3] Miller, J. B., "Nuclear quadrupole resonance detection of explosives: an overview," *Proc. SPIE* **8017**, 801715–801715–7 (2011).

[4] Suits, B. H., [*Handbook of Applied Solid State Spectroscopy*], 65–96, Springer US, Boston, MA (2006).

[5] Savukov, I., Seltzer, S., and Romalis, M., "Detection of NMR signals with a radio-frequency atomic magnetometer," *Journal of Magnetic Resonance* **185**(2), 214 – 220 (2007).

[6] Suits, B. H., "The noise immunity of gradiometer coils for ^{14}N NQR land mine detection: Practical limitations," *Applied Magnetic Resonance* **25**(3), 371–382 (2004).

[7] Cooper, R. J., Prescott, D. W., Matz, P., Sauer, K. L., Dural, N., Romalis, M. V., Foley, E. L., Kornack, T. W., Monti, M., and Okamitsu, J., "Atomic magnetometer multisensor array for rf interference mitigation and unshielded detection of nuclear quadrupole resonance," *Phys. Rev. Applied* **6**, 064014 (Dec 2016).

[8] *Twinleaf*. http://www.twinleaf.com/ (2014).

[9] Ramo, S., Whinnery, J. R., and Van Duzer, T. V., [*Fields and Waves in Communication Electronics*], Wiley (1994).

[10] Corney, A., [*Atomic and Laser Spectroscopy*], Oxford University Press, Oxford (1977).

[11] Alem, O., Sauer, K. L., and Romalis, M. V., "Spin damping in an rf atomic magnetometer," *Phys. Rev. A* **87**, 013413 (Jan 2013).

[12] Savukov, I. M., Seltzer, S. J., Romalis, M. V., and Sauer, K. L., "Tunable atomic magnetometer for detection of radio-frequency magnetic fields," *Phys. Rev. Lett.* **95**, 063004 (Aug 2005).

[13] Walker, T. G. and Happer, W., "Spin-exchange optical pumping of noble-gas nuclei," *Rev. Mod. Phys.* **69**, 629–642 (Apr 1997).

[14] Lee, S.-K., Sauer, K. L., Seltzer, S. J., Alem, O., and Romalis, M. V., "SubfemtoTesla radio-frequency atomic magnetometer for detection of nuclear quadrupole resonance," *Applied Physics Letters* **89**(21), – (2006).

[15] Malone, M. W., McGillvray, M., and Sauer, K. L., "Revealing dipolar coupling with NQR off-resonant pulsed spin locking," *Phys. Rev. B* **84**, 214430 (Dec 2011).